AN IMPROVED MODEL TO PREDICT NONUNIFORM DEFORMATION OF Zr-2.5 Nb PRESSURE TUBES

Q.M. Lei and H.Z. Fan
Atomic Energy of Canada Limited
Safety Thermalhydraulics Branch
Pinawa, Manitoba, Canada R0E 1L0

ABSTRACT

Present circular pressure-tube ballooning models in most fuel channel codes assume that the pressure tube remains circular during ballooning. This model provides adequate predictions of pressure-tube ballooning behaviour when the pressure tube (PT) and the calandria tube (CT) are concentric and when a small (<100°C) top-to-bottom circumferential temperature gradient is present on the pressure tube. However, nonconcentric ballooning is expected to occur under certain postulated CANDU® (CANada Deuterium Uranium) accident conditions. This circular geometry assumption prevents the model from accurately predicting nonuniform pressure-tube straining and local PT/CT contact when the pressure tube is subjected to a large circumferential temperature gradient and consequently deforms in a noncircular pattern. This paper describes an improved model that predicts noncircular pressure-tube deformation. Use of this model (once fully validated) will reduce uncertainties in the prediction of pressure-tube ballooning during a postulated loss-of-coolant accident (LOCA) in a CANDU reactor.

The noncircular deformation model considers a ring or cross-section of a pressure tube with unit axial length to calculate deformation in the radial and circumferential directions. The model keeps track of the thinning of the pressure-tube wall as well as the shape deviation from a reference circle. Such deviation is expressed in a cosine Fourier series for the lateral symmetry case. The coefficients of the series for the first m terms are calculated by solving a set of algebraic equations at each time step. The model also takes into account the effects of pressure-tube sag or bow on ballooning, using an input value of the offset distance between the centre of the calandria tube and the initial centre of the pressure tube for determining the position radius of the pressure tube.

One significant improvement realized in using the noncircular deformation model is a more accurate prediction in maximum pressure-tube strain and thus the likelihood of pressure-tube failure. Of 44 sets of comparisons, the agreement between the calculated and measured maximum pressure-tube strain has increased from 75% using the circular model to 95% using the noncircular model. The results show that the noncircular model is able to predict pressure-tube failure, local PT/CT contact, circumferential spread of the contact, and full circumferential contact. The work described in this paper was funded by the CANDU Owners Group (COG).

CANDU® is a registered trademark of Atomic Energy of Canada Limited (AECL).

1. INTRODUCTION

One of the postulated accident events in the licensing and safety assessment of CANDU reactors is a large-break LOCA. During such an event, coolant in the fuel channels downstream of a break can become stagnated. The coolant may boil off, causing the upper portion of the fuel bundles and pressure tube to become exposed to superheated steam while the lower portion remains in liquid. The temperature of the pressure tube will rise and vary circumferentially. If the primary heat transport system in the broken loops remains pressurized, the pressure tube may balloon into contact with the calandria tube, rejecting heat to the moderator. Whether or not the pressure tube ruptures prior to ballooning contact depends on the system pressure and the circumferential temperature gradients on the pressure tube [1]. Therefore, it is essential to predict the transient circumferential temperature gradients and the resultant nonuniform pressure tube deformation.

Small top-to-bottom circumferential temperature gradients will result in fairly uniform (and hence circular) deformation of the pressure tube. Large top-to-bottom circumferential temperature gradients will result in nonuniform (and hence noncircular) deformation of the pressure tube [2,3]. A circular pressure-tube ballooning model (GRAD) was developed by Shewfelt et al. [4] using the creep rate equations of Zr-2.5 Nb pressure tubes developed from uniaxial tests [5]. This model is used in most fuel channel codes such as FACTAR [6] and CATHENA [7] and assumes the pressure tube remains circular during ballooning. The circular model requires the pressure-tube circumference be divided into sectors. It keeps track of the sector circumferential length and wall thickness based on the temperature and stress calculated for each sector. A mean radius of the pressure tube is updated at each time step by summing all sector lengths and then dividing by π. This approach allows the model to predict nonuniform pressure-tube strain, but prevents the model from predicting local PT/CT contact because it assumes PT/CT contact occurs over the entire circumference simultaneously.

The circular deformation model predicts full circumferential PT/CT contact once the calculated total pressure-tube circumferential length reaches the value that is limited by the calandria tube. In reality, when the pressure tube is subjected to a large circumferential temperature gradient, it deforms in an egg-shaped pattern as observed from full scale pressure-tube ballooning experiments [1,2,3]. The hottest area (e.g., at the top) of the pressure tube may deform into contact with the calandria tube before the total pressure-tube circumferential length reaches the overall limit. When the circular model is applied to such scenarios, overestimations of pressure-tube wall thinning at the hottest location results.

The circular deformation model assumes that there is no change in the curvature of pressure-tube circumference regardless of circumferential temperature gradients on the pressure tube. The calculated mean radius of the pressure tube is used to estimate the hoop stress of each sector. This results in overestimating the hoop stress (hence the hoop strain) at locations where the circumferential temperature gradient is large, resulting in a reduction of the local curvature of pressure-tube circumference.

The circular deformation model has been assessed extensively using data from full scale pressure-tube ballooning experiments [2,3,8,9]. The model was shown to accurately predict the pressure-

tube ballooning behaviour when a small top-to-bottom circumferential temperature gradient (<100°C) was present on the pressure tube. A majority of calculated results, however, indicated that the circular model overestimated maximum pressure-tube strain when a large circumferential temperature gradient developed on the pressure tube.

The previous assessments using experimental data indicate there is a need to remove the circular geometry assumption from the pressure-tube ballooning model when large circumferential temperature gradients develop on the pressure tube and when the pressure tube sags or bows inside its surrounding calandria tube. This paper describes a noncircular Pressure-Tube RING (PTRING) deformation model that resulted from modifications to a ring deformation model of Shewfelt [10]. Comparisons of the PTRING results with the experimental results and with the circular model results are also reported. The goal of this work is to provide a validated model to improve accuracy in the prediction of noncircular pressure-tube ballooning during a postulated LOCA.

2. DESCRIPTION OF THE NONCIRCULAR MODEL

The pressure tube is assumed to be in an original cylindrical shape. An elemental ring of the tube being considered is taken far from the ends and any supports (Figure 1a) to eliminate axial loading effects. The difference, p, between the internal and external pressures on the tube is assumed to be uniform over the tube surface, and can be a function of time. At a given time, p is assumed to normally act on the mid-surface (between the inner and outer surfaces) of the tube. The pressure will result in extension of this mid-surface in the hoop direction. The hoop bending moment on the ring, however, is assumed to result in no extension of this mid-surface, i.e., inextensible bending deformation as defined by Timoshenko and Gere [11]. The effect of axial temperature variation on creep deformation is assumed to be negligible compared to that of the circumferential temperature variation. Thus, the longitudinal bending and twisting moments are neglected.

Figure 1b shows the polar coordinates on the pressure-tube ring. Any point "P" on the ring can be described by a position radius, ρ, and the central angle, α, where $\alpha=0$ is the vertical symmetric line passing the centre of the ring, and $\rho=\rho(\alpha)$. The origin of the coordinates (ρ,α) is at the centre of the calandria tube (Figure 1c). The initial centre of the pressure-tube ring is assumed to be on the vertical symmetric line and have an offset, e, with respect to the centre of the calandria tube. The offset value is positive when the pressure-tube centre is below the calandria-tube centre, zero when the two tubes are concentric, and negative when the pressure-tube centre is above the calandria-tube centre. The pressure-tube ring can be located using a reference circle with a mean radius, R, and the deviations from the mean radius. The centre of the reference circle may not be fixed during nonuniform deformation but remains on the vertical symmetric line. The reference or central angle, θ, is based on the reference circle. The curvature of the ring is described by the radius of curvature, r. Only when the ring is circular is the radius of curvature of the ring equal to the position radius, i.e., $r=\rho$.

The ratio of wall thickness, t, to the radius of curvature is assumed to be much smaller than unity (e.g., $t/r<0.1$ [12]). Hence, the shell theorem [13] can be applied to the ring. Only hoop stress, σ,

is considered since the radial and shear stresses are assumed to be negligibly small. Within each time step, the effects of creep and pressure loading are considered in two interrelated steps:

(1) The effect of high-temperature creep with the hoop stress is assumed to cause the pressure-tube ring to diametrically deform. A mean radius of the ring is estimated, which represents a reference circular shape of the ring at the time considered. This step employs the approach similar to that used in the current circular pressure-tube deformation model [4].

(2) The deviation from the reference circular shape is determined by assuming bending deformation caused by changes in hoop bending stiffness due to circumferential temperature gradients. This step solves a set of algebraic equations to obtain the first m terms of a cosine Fourier series for determining the radial displacement as a function of circumferential angle.

2.1 Determination of the Mean Radius

The mean radius of the reference circle, R, can be calculated by

$$R = R_1 + \frac{1}{\pi}\int_0^{\pi} (d\varepsilon / d\tau)\Delta\tau\, R_1\, d\theta \qquad (1)$$

where $\Delta\tau$ is the current time interval, R_1 is the mean radius of the ring at τ-$\Delta\tau$, and $d\varepsilon/d\tau$ is the creep rate. The creep rate, calculated using Shewfelt's creep rate correlations [5], is a function of hoop stress, temperature, and time. The hoop stress can be statically determined by $\sigma=p\,r/t$. In the circular model, σ is estimated using the mean radius, R, of the tube. In this noncircular model, the linkage of σ with the radius of curvature of the ring, r, better represents stress changes with changing geometry. Once the creep rate at a circumferential location is calculated, the wall thickness of the ring at this location is updated using the assumption of volume conservation that is given by $t=t_1/[1+(d\varepsilon/d\tau)\Delta\tau]$, where t_1 is the wall thickness at τ-$\Delta\tau$.

2.2 Determination of Deviation from the Mean Radius

At a given time, the shape of the ring can be described by the mean radius of the ring, R, and two displacements: the radial displacement $w(\theta)$ and the circumferential displacement $v(\theta)$. The radial displacement w is zero on the mean circle and taken as positive when it is directed away from the centre of the ring, and v is positive in the positive θ direction. Both w and v consist of two components due to hoop tension and hoop bending. For a pressure tube ring, hoop tension has a small influence on the shape deviation of the ring. Significant deviation from the reference circle can develop as a result of hoop bending even though the bending moment may result in a small fraction of hoop stress. This is because the bending stiffness of the ring is very small. Therefore, the shape deviation of the ring is assumed to be a result of hoop bending only.

For inextensible deformation of an internally pressurized ring, the relation between the bending moment and the radial displacement is given by Timoshenko and Gere [11]:

$$w'' + (w + w_0) = \frac{R^2}{E^* I} M \tag{2}$$

where w'' is the second derivative of w with respect to θ, w_0 is an average radial displacement due to hoop tension and high-temperature creep, E^* is the Young's modulus for the plane strain case, I is the moment of inertia of the cross section of the ring per unit axial length ($I=t^3/12$), and M is the hoop bending moment which is a function of θ and taken to be positive when it tends to decrease the curvature of the ring. The radial displacement w_0 is assumed to be (R-R_0), where R_0 is the initial mean radius of the ring. Also, $E^* = E/(1-\nu^2)$, where ν is the Possion's ratio, E=97200-68.3T, and temperature T is in °C [10].

Using the Young's modulus, equation 2 provides an approximate relationship between the curvature change and the bending moment on the pressure tube ring. In consideration of creep and deformation history, the bending stress (much smaller than the mean hoop stress) can be relaxed as the nonlinear stress-strain relationship exists. This effect was estimated during this study and found to have a small impact on the calculation of pressure-tube strain and position radius. Therefore, equation 2 is used to model noncircular pressure-tube deformation until first PT/CT contact occurs. After first contact, this equation is no longer applicable and thus a numerical scheme for deformation of the noncontact pressure-tube portion is employed (Section 2.4).

The nonlinear relation between the hoop tension force N and the shape deviation w can be approximated by [11]

$$N = (p + p^*) R = p\,(R + w'' + w) \tag{3}$$

where p^* is a distributed fictitious pressure load acting radially towards the centre of the ring. Note that $(w''+w)/R^2$ represents the change of curvature of the ring. When the curvature change is small, N is approximately equal to the membrane force, $p\,R$. After the solution of w is found, N is updated and then the hoop stress σ is calculated by N/t.

Since equation 2 can not be solved directly, the energy method is used for a set of algebraic equations to be solved for $w(\theta)$. The total strain energy being considered consists of the strain energy due to hoop bending and the strain energy due to hoop tension. The latter is a large fraction of the total strain energy. The increment of the mean radius from the initial radius, w_0, reflects the strain energy due to hoop tension (i.e., the effect of the hoop force N and creep). The strain energy due to hoop tension, however, is not affected by the deviation, $w(\theta)$, of the mean radius. Therefore, for determining $w(\theta)$, the strain energy, U_e, of the elastic bending deformation and the external energy, E_e, of the loads are expressed as

$$U_e = \int \frac{M^2}{2E^* I} ds = \int \frac{E^* I}{2R^4} (w'' + w + w_0)^2 \, ds \tag{4}$$

$$E_e = \int (p\, w_0 + p^*\, w)\, ds \tag{5}$$

The integration is along the half ring for the lateral symmetric case ($ds = R\, d\theta$, θ from 0 to π). There may be bending moments and tension forces acting at the ends ($\theta=0$ and $\theta=\pi$). Due to symmetry, there are no rotation and hoop displacements at the ends. Hence, such end section forces make no contribution in equation 5. The radial displacement $w(\theta)$ and its derivatives are assumed to be small compared with the mean radius R and must be a period function of 2π to meet a continuous geometry requirement. In general, $w(\theta)$ can be represented by a trigonometric series for thin-walled tube hoop bending problems [10,12]. For the symmetry case, $w(\theta)$ in the above energy expressions can be described by the cosine Fourier series:

$$w(\theta) = \sum_{n=2,3,\ldots} w_n \cos n\theta \tag{6}$$

Equation 6 excludes the constant term because of inextensible bending. The $w_1 \cos\theta$ term is also dropped because it just represents a rigid body movement in plane which could be determined by a reference condition (Section 2.3) rather than deformation equations. The coefficients of $w(\theta)$ can be determined by minimizing the potential energy [11], P_e , where $P_e = U_e - E_e$. This minimization takes the form of $\partial P_e / \partial w_k = 0$, where $k \geq 2$. Performing the differentiation gives

$$\int \frac{E^* I}{R^3} (w'' + w + w_0)(1 - k^2) \cos k\theta\, d\theta = (E_e)_{nk} \tag{7}$$

The left term of equation 7 has been obtained by differentiating equation 4 while w and w'' are obtained from equation 6. The integer k in equation 7 corresponds to the result of the differentiation with respect to w_k. The displacement w together with its second derivative w'' in equation 7 is still expressed by equation 6 with the integer n representing w_n in the series. The right term of equation 7 is the result of differentiation of equation 5 while p* is treated as the outcome of noncircular deformation and, therefore, has no variation with w when the energy method is used. Using the relation given in equation 3 and the orthogonality property of $\int \cos k\theta \cos n\theta\, d\theta = 0$ for $n \neq k$ renders $(E_e)_{nk} = 0$ for $n \neq k$ and $(E_e)_{nk} = (\pi/2) p (1 - k^2) w_k$ for $n = k$. If the first m terms of the cosine series are sufficient to represent $w(\theta)$, a set of algebraic equations for coefficients w_n can be established as

$$A_{kn}\, w_n = B_k \qquad (k = 2,3,\ldots,m; \quad n = 2,3,\ldots,m) \tag{8}$$

where,

$$A_{kn} = \int \frac{E^* I}{R^3} (1 - k^2)(1 - n^2) \cos n\theta\, \cos k\theta\, d\theta \qquad (k \neq n)$$

$$A_{kk} = \int \frac{E^* I}{R^3} (1 - k^2)^2\, \cos^2 k\theta\, d\theta + \frac{\pi}{2} p (k^2 - 1) \qquad (k = n)$$

$$B_k = \int \frac{E^* I}{R^3} w_0 \, (k^2 - 1) \cos k\theta \, d\theta$$

There are m-1 independent equations for m-1 unknowns, that is, w_2 to w_m. The diagonal terms of A_{kk} in the coefficient matrix are always positive. For a special case where the bending stiffness, $E^* I$, is uniform on the ring, A_{kn} and B_k will all be zero except for A_{kk}. Therefore, only zero solutions for w_n are obtained, signifying no shape deviation from the mean radius of the ring. This expected outcome indicates that the pressure tube ring is ballooning uniformly. If the original shape of the ring is circular and with a uniform thickness, the ring will remain circular during ballooning. When the pressure tube ring is subjected to a circumferential temperature gradient, the bending stiffness varies along the ring and non-zero solutions for w_n are obtained. Since the total increment of the mean radius (w_0=R-R_0) is used on the right side of equation 8, the solutions for w_n represent the total radial displacements at time τ. Also note that, as both terms in A_{kk} are positive, the effect of the tension force or internal pressure tends to reduce the degree of the shape deviation.

2.3 Position Radius

Any point on the pressure-tube ring can be located by the position radius $\rho(\alpha)$. At time τ, $\rho(\alpha)$ can be determined using the initial offset distance e between the pressure tube and the calandria tube, the current mean radius R, and the current radial displacement $w(\theta)$ plus the first term $w_1 \cos\theta$ that has been excluded in equation 6. The coefficient w_1 is the vertical distance between the centre of the currently calculated reference circle and the centre of the initial ring. If a uniform temperature develops on the ring, it balloons uniformly and the centre of the currently calculated reference circle coincides with the centre of the initial ring. If a circumferential temperature gradient develops on the ring, nonuniform ballooning occurs and the centre of the currently calculated reference circle "floats" on the vertical symmetric line. If there is not a large cold (temperatures below 500°C) region on the ring where local creep is negligible, the rigid body movement relative to the centre of gravity of the ring must be zero. For this scenario, the coefficient w_1 is determined by calculating the vertical distance between the centre of the reference circle and the centre of gravity of the ring. If there exists a large cold region on the ring, the known displacement of the cold region is used to determine w_1. After w_1 is obtained, the true radial displacement $w^*(\theta)$, including the initial offset e, is given by

$$w^*(\theta) = (w_1 - e)\cos\theta + w(\theta) = (w_1 - e)\cos\theta + \sum_{n=2,3,..m} w_n \cos n\theta \qquad (9)$$

The true circumferential displacement $v^*(\theta)$ can be obtained using the approximate relation of $w^*(\theta)+dv^*/d\theta=0$. The position (ρ,α) of a point on the ring, relative to the centre of the calandria tube, is given by

$$\rho = \left[(R + w^*)^2 + (v^*)^2\right]^{1/2}; \qquad \alpha = \theta + \sin^{-1}(v^* / \rho) \qquad (10)$$

2.4 Approximation after First Contact

Local PT/CT contact is indicated by $\rho+t/2 \geq R_c$, where R_c is the inner radius of the calandria tube. The calandria tube is assumed to undertake no deformation following pressure-tube contact. Therefore, the pressure-tube ring in the contact region has no further radial displacement and wall thickness reduction. Prior to full circumferential contact, deformation of the noncontact pressure-tube portion after first contact is a complex problem. The above equations are no longer applicable for the pressure tube that has partially contacted its calandria tube.

For completeness of this ring deformation model, a simple numerical scheme is adopted to model the continued deformation of the noncontact pressure-tube portion after first contact is predicted. It assumes there is no further pressure-tube circumferential length increase for the contact region and the creep strain increment of a noncontact region during a time step results in an increment in the position radius of this noncontact region. This numerical scheme is similar to that used in the circular deformation model. This approach approximately models the propagation of contact and adequately calculates pressure-tube strain following first contact.

2.5 Numerical Implementation

The noncircular pressure-tube deformation model described above has been numerically implemented into a stand-alone computer program PTRING. During each time step, the matrix equation (equation 8) is directly solved for w_n using Gauss's elimination method. The number of terms (order up to m) included in the cosine series (equation 6) is decided so that the error in $w(\theta)$ is less than 1%. The lower bound failure criterion [4] is used to predict pressure-tube failure due to local necking. The upper bound failure criterion [4] is currently not available in PTRING but will be added in the future.

Half of the pressure-tube circumference is divided into sectors. Each sector is further divided into subsectors for increasing accuracy in the strain calculation. Figure 2 shows the influence of the total number of sectors used on PTRING results under two different test conditions. In general, it is recommended that at least 10 sectors be used for a half pressure-tube circumference with each sector being divided into 10 subsectors when PTRING is used to model noncircular pressure-tube deformation.

3. COMPARISON WITH THE CIRCULAR MODEL

A numerical test is used here to compare the PTRING results with the results from the circular model GRAD. A pressure tube is internally pressurized at 1 MPa and is initially concentric inside a calandria tube. A time-independent, cosine temperature profile expressed as $T(\theta)=200+300(1+\cos\theta)$ is imposed on the pressure tube. Figure 3 shows the pressure-tube geometries and wall thicknesses predicted by PTRING and GRAD at two sample times. At 53.7 s, PTRING predicted PT/CT contact at the top with an egg-shaped geometry for the deforming pressure tube. At this time, GRAD predicted a circular geometry for the pressure tube with an increase of 8.5% in its outer radius. GRAD predicted full circumferential PT/CT contact at 73.8 s, 20.1 s after PTRING predicted first contact at the top of the pressure tube. At this

time, PTRING did not predict full circumferential contact and the predicted pressure-tube geometry remained noncircular. The wall thicknesses on the upper half of the pressure tube predicted by PTRING were thicker than those by GRAD. The difference came from two effects. The effect of changing pressure-tube curvature was taken into account in the stress calculation in PTRING, but not in GRAD. Local PT/CT contact at the top was predicted by PTRING, but GRAD could only predict full circumferential contact. Under these test conditions, PTRING is believed to provide a more accurate prediction of pressure-tube deformation.

4. VALIDATION USING PRESSURE-TUBE BALLOONING DATA

This section describes an assessment of the noncircular pressure-tube deformation model using data from full scale pressure-tube ballooning experiments. Measured transient pressure-tube temperatures and pressures were input to PTRING. A half pressure-tube circumference was uniformly divided into 18 sectors (with 10 subsectors in each sector). At circumferential locations where measured temperatures were not available, linear interpolation was performed to obtain the pressure-tube temperatures.

4.1 Pressure Tube Ballooning without Pressure Tube Offset

Data from one of the Pressure Tube Circumferential Temperature Distribution Experiments, PTΔT S-1-4 [1], were used in this study to assess PTRING under conditions of a concentric PT/CT geometry and a large circumferential temperature gradient on the pressure tube. The horizontal test section consisted of a 2600-mm-long section of autoclaved Zr-2.5 Nb pressure tube sealed at one end and concentrically mounted inside a 2300-mm-long Zr-2 calandria tube. Thirty-seven fuel element simulators were arranged to represent a CANDU fuel bundle. The heated length was 2300 mm. Ten thermocouples were installed around the pressure-tube outside surface at each of three axial locations.

At the beginning of the experiment, the pressure tube was filled with water and pressurized to 4 MPa. Once the temperature of water in the pressure tube was raised to the saturation temperature, the experiment started by opening a steam exit valve at one end of the test section, allowing water in the pressure tube to boil off. This coolant boil-off resulted in a large top-to-bottom circumferential temperature gradient (as high as 464°C) on the pressure tube. Figure 4a shows the histories of the measured pressure-tube temperatures at axial location 2. The thermocouple traces indicate that the pressure-tube top had an initial contact with the calandria tube at 864 s, and that there was no full circumferential contact in the experiment. At 1171 s, the test-section pressure was decreased and no further pressure-tube straining occurred thereafter.

The measured temperature transients were input to PTRING to perform the deformation calculation. The noncircular model correctly predicted initial PT/CT contact at the top of pressure tube. The predicted contact time was 867.3 s, 3.3 s later than in the experiment. At the end of the experiment (1200 s), the calculated total pressure-tube strain (circumferential length increment) was 10.0%. The predicted contact area was ±73 deg over the top of the calandria tube, which agrees with the contact area indicated by the traces of the top four thermocouples

(Figure 4a). When the circular deformation model in CATHENA MOD-3.5/Rev 0 was used, no PT/CT contact was predicted. The calculated total pressure-tube strain at the end of the experiment was 14.7%.

Figure 4b shows the predicted pressure-tube wall thicknesses at the end of the calculation with the post-test measured values. Both the circular and noncircular model results at 1200 s are shown. The calculated wall thicknesses using the noncircular model (solid line) follow the measured data ('Δ' symbol) closely, indicating PTRING accurately calculated the maximum pressure-tube strain at the top and the strain variation around the pressure tube circumference. The calculated pressure-tube wall thicknesses using the circular model were within ±20% of the experimental data, which was deemed to be within experimental uncertainties. The pressure-tube wall thinning at the top was overestimated significantly (by 18%) using the circular model.

4.2 Ballooning of an Initially Offset Pressure Tube

Data from PTΔT test S-5-1 [2] were used to validate PTRING under conditions where the pressure tube was initially offset inside the calandria tube and subjected to a large circumferential temperature gradient. In this test, the horizontal test section consisted of a 28 fuel-element-simulator bundle. The length of the heated zone was 1800 mm. The bundle was surrounded by a 2105-mm-long pressure tube mounted inside a 1780-mm-long calandria tube. The test-section pressure was 4 MPa. The pressure tube was offset by 3.6 mm in the calandria tube to simulate a sagged pressure tube. The pressure-tube temperatures were monitored at five distinct axial locations, with a maximum recorded top-to-bottom circumferential temperature gradient of 475°C. Local PT/CT contact was observed along the test section. The pressure tube did not fail in this experiment.

The measured pressure-tube temperatures at axial location 1 (225 mm from the closed end) are shown in Figure 5a. At 714.3 s, the pressure-tube top had contacted the calandria tube. The temperature traces of thermocouples 2, 3, 8 and 7 after 714.3 s indicate that contact spread from the top to the side of the pressure tube within 10 s. The temperature traces of the thermocouples around the bottom half of the pressure tube did not show any contact during the experiment.

Two calculations were performed using PTRING to show the effects of pressure-tube offset on ballooning. In one calculation, the pressure tube offset was neglected and an initial concentric PT/CT geometry (zero offset) was used. In the other calculation, the experimental pressure-tube offset of 3.6 mm was used. The noncircular model predicted initial PT/CT contact at 713.0 s for the concentric case and at 714.7 s for the offset case. Both the predicted times agreed with the experimental time of 714.3 s, with the predicted time for the offset case being closer to the experimental time. For the channel pressure of 4 MPa in this test, the pressure-tube offset value of 3.6 mm had a minor impact on the predicted initial contact time (causing a 1.7-s difference). This offset, however, had a much greater impact on the predicted pressure-tube wall thickness reduction, as shown in Figure 5b. When the effects of pressure-tube offset were included, the noncircular model accurately predicted the minimum pressure-tube wall thickness that occurred 20 deg from the top of the pressure tube. When the offset effects were not included, the wall thickness reduction at this location was underestimated. The predicted contact area by the

noncircular model with the inclusion of pressure-tube offset effects was ±81 deg at the top of the channel, which agreed with the contact area inferred from the thermocouple traces in Figure 5a.

The circular model did not account for pressure-tube offset effects and could not predict local PT/CT contact. Under these test conditions, the circular model predicted neither PT/CT contact nor pressure-tube rupture. The predicted pressure-tube wall thicknesses, however, were in agreement with the measured values as well as with the results predicted by the noncircular model with the inclusion of pressure-tube offset effects.

4.3 Pressure Tube Ballooning at 10 MPa

Data from a 10-MPa pressure-tube ballooning experiment were used in this study to determine if PTRING could predict the observed pressure-tube failure. Temperatures of the pressure tube, measured at the mid-plane of the pressure-tube wall, are shown in Figure 6a. As the pressure tube was heated, a circumferential temperature gradient of 200°C developed. As a result, the pressure tube deformed and ruptured at the top at 898 s, before any PT/CT contact occurred. Using the measured temperatures, both the circular and noncircular deformation models predicted rupture of the pressure tube due to a local break (lower bound criterion on failure with a wall defect assumed to be 13 μm). The predicted rupture time was 892 s, which was 6 s earlier than the experiment.

4.4 PTRING Validation Results Summary

Presented above are 3 of the 44 sets of measured and calculated results. In this study, forty-four sets of data from various full scale fuel channel experiments were used, covering internal pressures from 1 to 10 MPa and top-to-bottom circumferential temperature gradients as high as 690°C. Using measured pressure-tube circumferential temperature distributions, PTRING correctly predicted PT/CT contact that initially occurred at the hottest location around the pressure tube. Figure 7a shows that, of 22 cases where initial contact occurred in the experiments, the predicted initial contact times for 14 cases were within ±10 s of the experimental times. For the remaining 8 cases, PTRING did not predict local PT/CT contact. An assessment was performed to determine how much longer PTRING would need to predict PT/CT contact. Less than 10 s more was needed for PTRING to predict PT/CT contact for each of the 8 cases when the measured pressure-tube temperatures were extrapolated beyond the time of contact. Figure 7a also shows that the predicted pressure-tube failure and full PT/CT contact times were within ±8 s of the experimental times.

The calculated pressure-tube wall thicknesses that fall within ±20% of the measured data were considered to be within the experimental uncertainties based on an uncertainty analysis performed in this study. Using this criterion, the agreement between the calculated and post-test measured minimum pressure-tube wall thicknesses increased from 75% using the circular model (Figure 7c) to 95% using the noncircular model (Figure 7b). Two of these calculated results were largely influenced by thermocouple failure during ballooning in the experiments and thus underestimated pressure-tube wall thinning significantly.

The noncircular model was also shown to be capable of predicting the circumferential spread of PT/CT contact following initial contact. A majority of the calculated PT/CT contact areas were within ±30% of the experimentally inferred areas at the end of each experiment. The ability of PTRING to predict PT/CT contact areas during pressure-tube ballooning can be utilized to improve the estimation of the heat load to the moderator following PT/CT contact.

5. CONCLUSIONS

A noncircular deformation model for Zr-2.5 Nb pressure tubes has been analytically developed and numerically implemented into a stand-alone computer program PTRING. Forty-four sets of data from various full scale fuel channel experiments have been used to validate PTRING and evaluate improvements in modelling pressure-tube behaviour by comparing the noncircular model results with the circular model results. One of the significant improvements in using the noncircular deformation model is a more accurate prediction in maximum pressure-tube strain and thus the likelihood of pressure-tube failure when large circumferential temperature gradients develop on the pressure tube and/or when the pressure tube is initially offset inside the calandria tube. The results have also showed the ability of PTRING to predict pressure-tube failure, local PT/CT contact, circumferential spread of the contact, and full circumferential contact. Further validation of this noncircular pressure-tube deformation model using experimental data with channel pressures between 1.5 and 3.5 MPa and high pressures above 6 MPa is recommended. Use of this model, once fully validated, will reduce uncertainties in the prediction of pressure-tube ballooning during a postulated LOCA.

REFERENCES

(1) SO, C.S., GILLESPIE, G.E., MOYER, R.G. and LITKE, D.G., "The Experimental Determination of Circumferential Temperature Distributions Developed in Pressure Tubes during Slow Coolant Boildown," Proceedings of the 8th Annual CNS Conference, Saint John, NB, pp. 241-248, 1987.

(2) LEI, Q.M., SANDERSON, D.B., SWANSON, M.L., WALTERS, G.A. and ROSINGER, H.E., "Experimental and Theoretical Investigation of Pressure Tube Circumferential Temperature Gradients during Coolant Boil-Off," Proceedings of the 13th Annual CNS Conference, Saint John, NB, 1992.

(3) LEI, Q.M., GOODMAN, T.M. and SANDERSON, D.B., "Modelling Thermalhydraulic/Thermal-Mechanical Behaviour of a Fuel Channel with Stratified Two-Phase Flow Using CATHENA," Proceedings of the 5th International Conference on Simulation Methods in Nuclear Engineering, Montreal, PQ, 1996.

(4) SHEWFELT, R.S.W. and GODIN, D.P., "Verification Tests for GRAD, a Computer Program to Predict Nonuniform Deformation and Failure of Zr-2.5 wt% Nb Pressure

Tubes during a Postulated Loss-of-Coolant Accident," Atomic Energy of Canada Limited Report, AECL-8384, 1985.

(5) SHEWFELT, R.S.W., LYALL, L.W. and GODIN, D.P., "A High-Temperature Creep Model for Zr-2.5 wt% Nb Pressure Tubes," Journal of Nuclear Materials, 125, pp. 228-235, 1984.

(6) WESTBYE, C.J., BRITO, A.C., MACKINNON, J.C., SILLS, H.E. and LANGMAN, V.J., "Development, Verification and Validation of the Fuel Channel Behaviour Computer Code FACTAR," Proceedings of 16th Annual CNS Conference, Saskatoon, SK, Vol. II, 1995.

(7) RICHARDS, D.J., HANNA, B.N., HOBSON, N. and ARDRON, K.H., "CATHENA: A Two-Fluid Code for CANDU LOCA Analysis, (renamed from ATHENA)," Presented at the 3rd International Topical Meeting on Reactor Thermalhydraulics, Newport, RI, 1985.

(8) MUIR, W.C. and BAYOUMI, M.H., "Prediction of Pressure Tube Ballooning under Non-Uniform Circumferential Temperature Gradients and High Internal Pressure," Proceedings of the 5th International Conference on Simulation Methods in Nuclear Engineering, Montreal, PQ, 1996.

(9) MUIR, W.C. and BAYOUMI, M.H., "Simulation and Analysis of the Thermal and Deformation Behaviour of 'As-Received' and 'Hydrided' Pressure Tubes Used in the Circumferential Temperature Distribution Experiments (End of Life/Pressure Tube Behaviour)," Proceedings of 16th Annual CNS Conference, Saskatoon, SK, Vol. II, 1995.

(10) SHEWFELT, R.S.W., "Ballooning of Thin-Walled Tubes with an Azimuthal Temperature Gradient," Atomic Energy of Canada Limited Report, AECL-7799, 1983.

(11) TIMOSHENKO, S.P. and GERE, J.M., "Theory of Elastic Stability," McGraw-Hill Book Company, New York, 1961.

(12) ONG, L.S., "Allowable Shape Deviation in a Pressurized Cylinder," Journal of Pressure Vessel Technology, Vol. 116, pp. 274-277, 1994.

(13) FLUGGE, W., "Stresses in Shell," Springer-Verlag, New York, 1966.

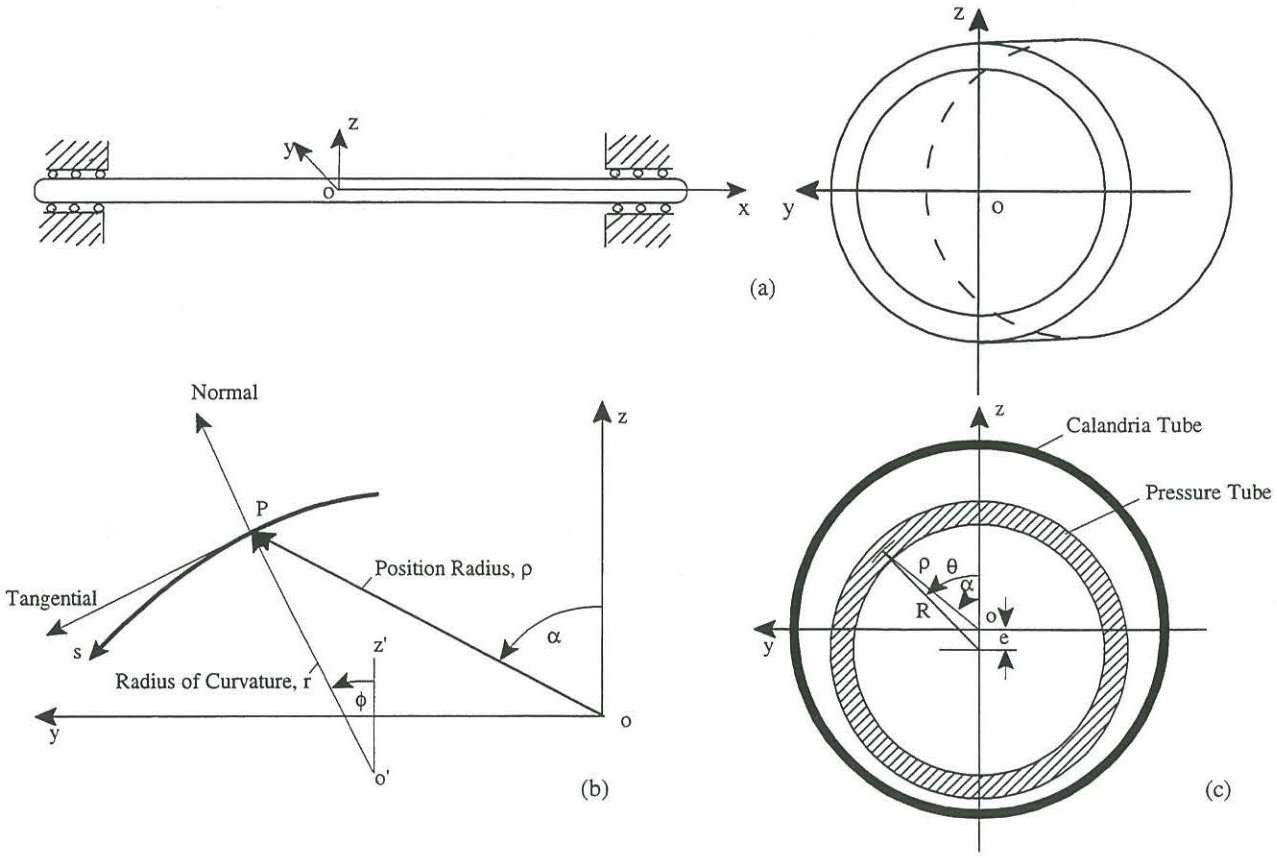

FIGURE 1: Elemental Ring of the Pressure Tube (a), Two Coordinates on the Ring (b) and the Initial Ring Position in the Calandria Tube (c)

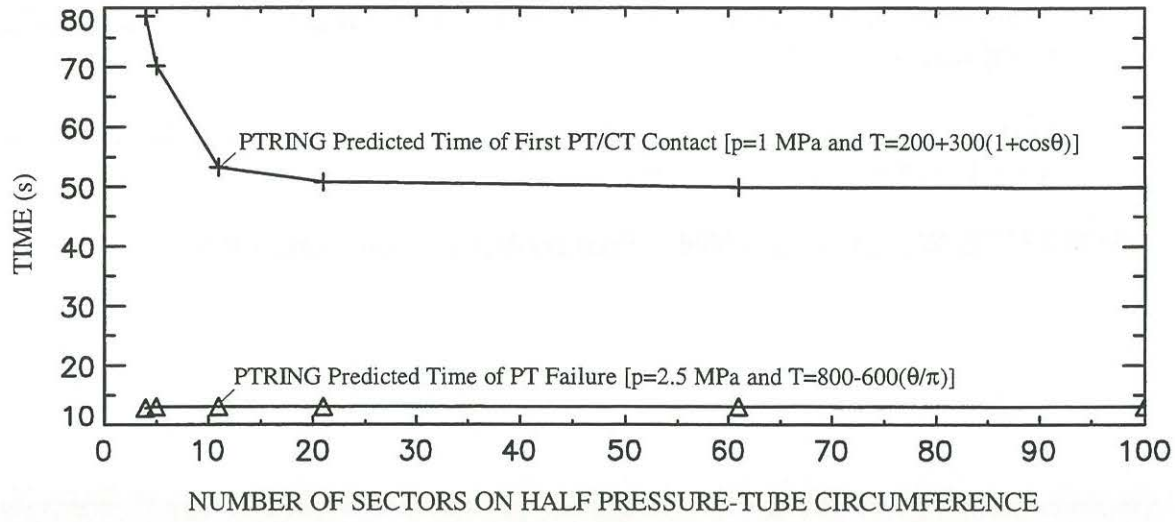

FIGURE 2: Influence of Total Number of Sectors on PTRING Results in Two Numerical Tests (Each Sector was Divided into 10 Subsectors in PTRING)

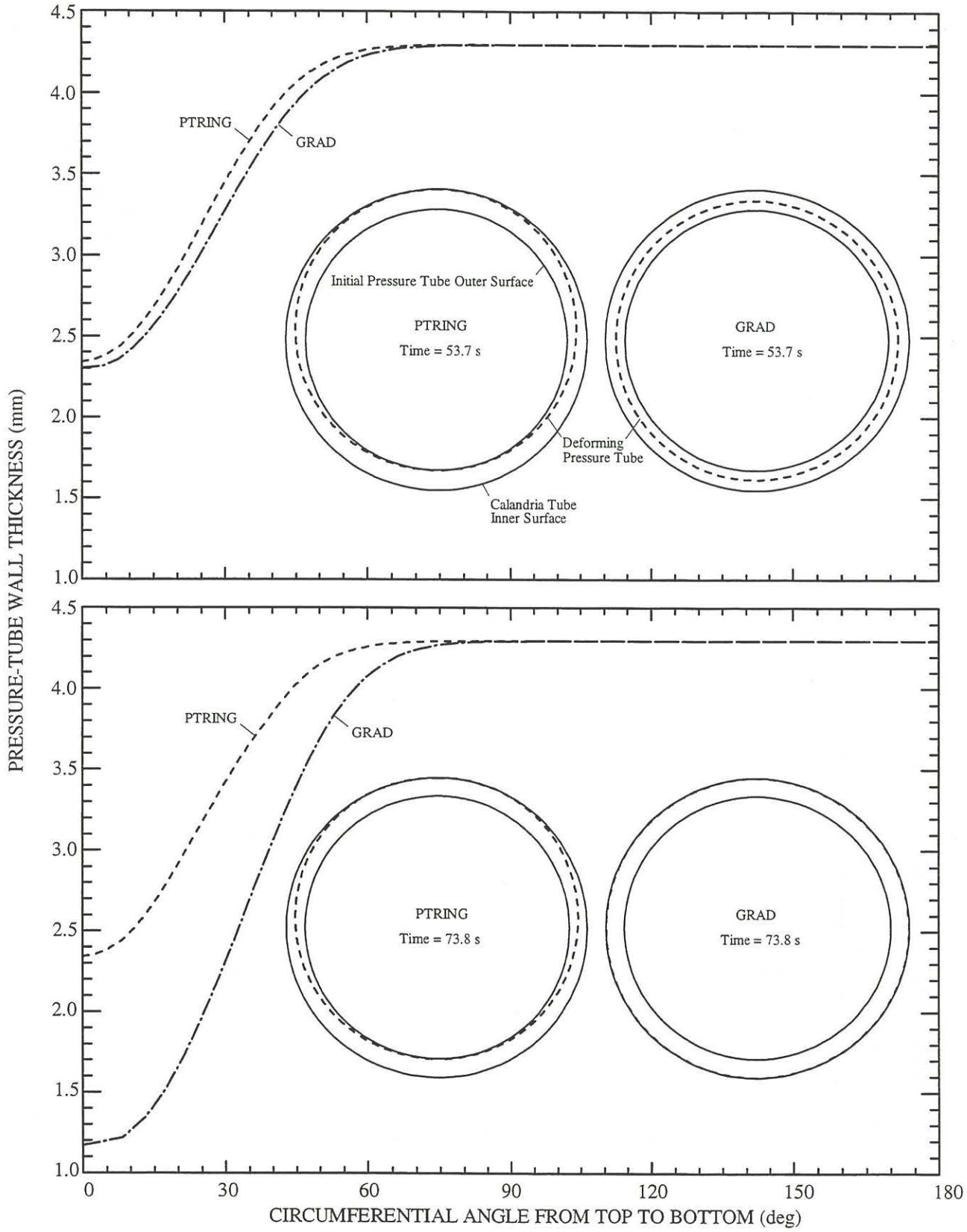

FIGURE 3: Comparison Between the Circular and Noncircular Models on Predicted Pressure-Tube Geometry and Circumferential Wall Thickness Distribution at Two Different Times (T=200+300(1+cosθ); p=1 MPa)

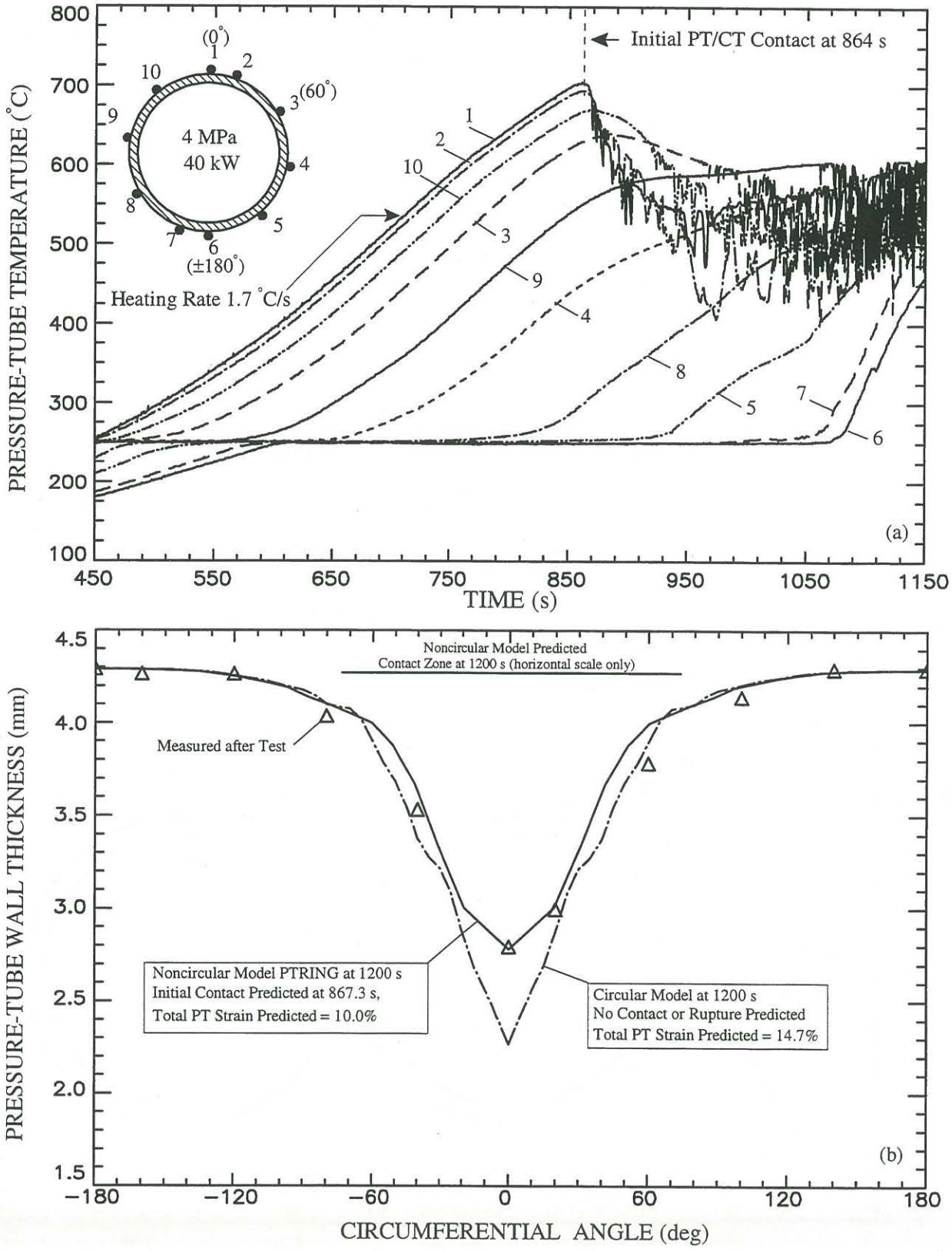

FIGURE 4: Measured Pressure-Tube Outer-Surface Temperatures (a) and Measured and Predicted Pressure-Tube Wall Thicknesses (b) at Axial Location 2 of PTΔT Test S-1-4

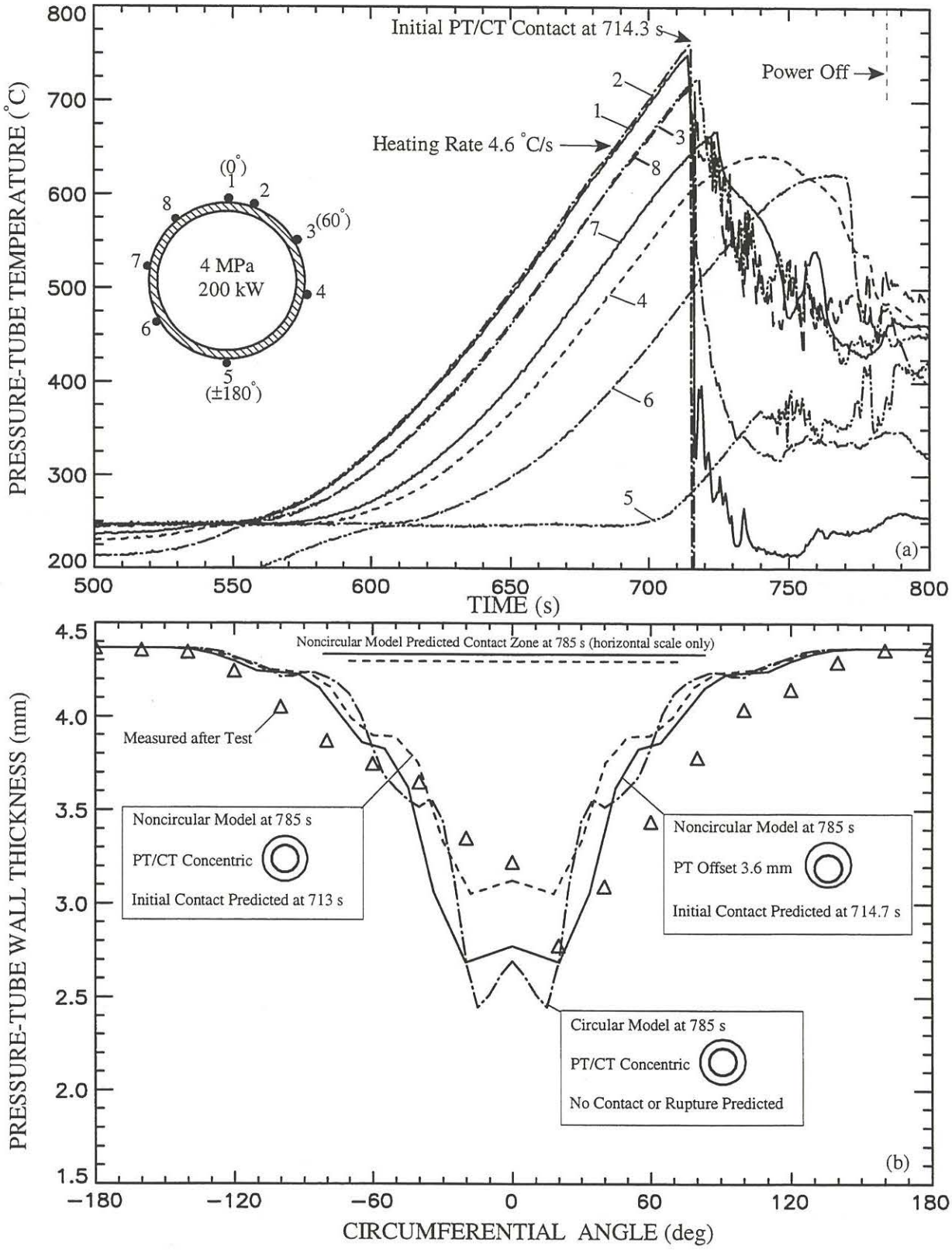

FIGURE 5: Measured Pressure-Tube Outer-Surface Temperatures (a) and Measured and Predicted Pressure-Tube Wall Thicknesses (b) at Axial Location 1 of PTΔT Test S-5-1

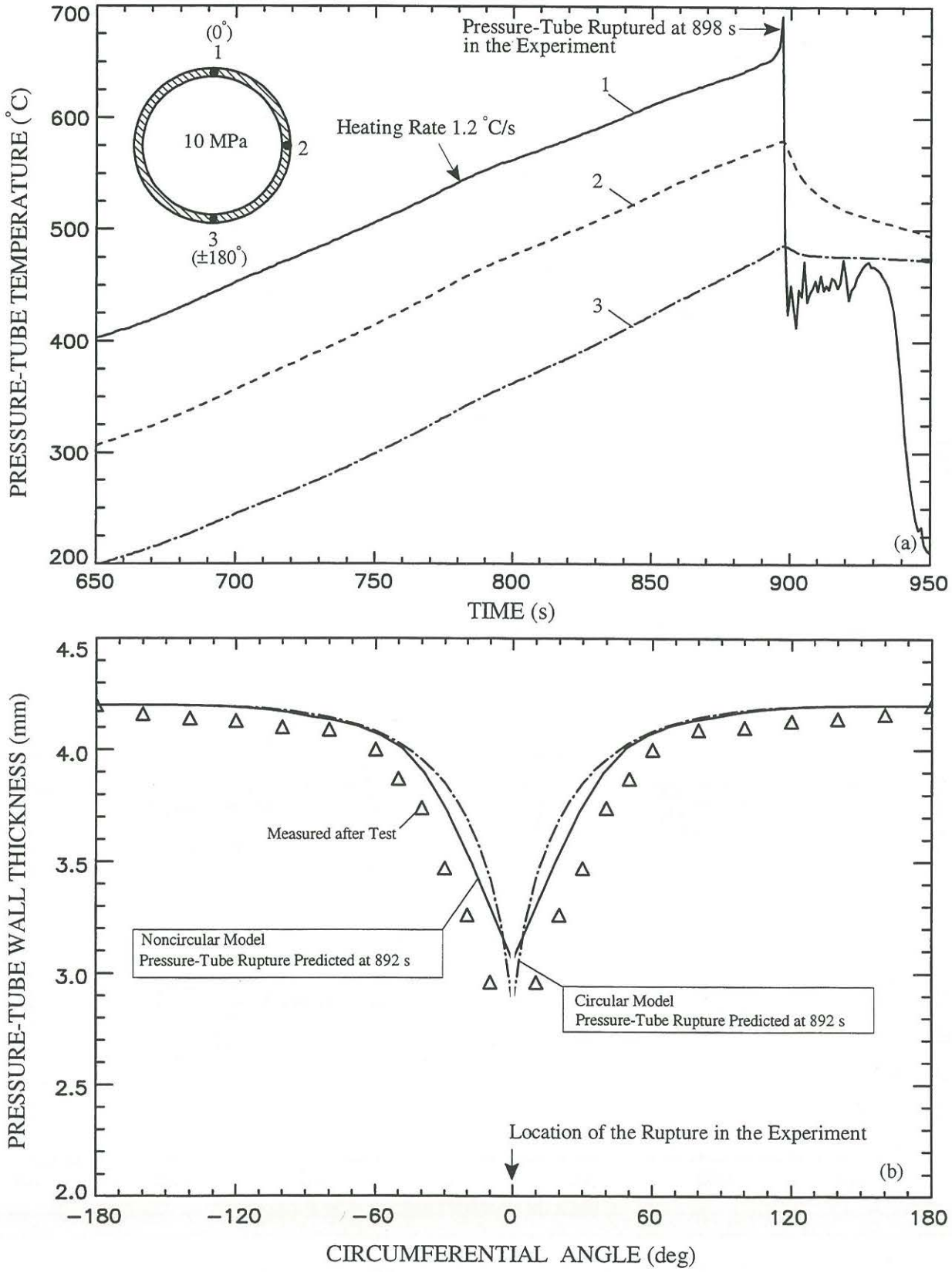

FIGURE 6: Measured Temperatures (a) and Measured and Predicted Wall Thicknesses (b) of the Pressure Tube for the Contact Boiling Experiment HPHT3

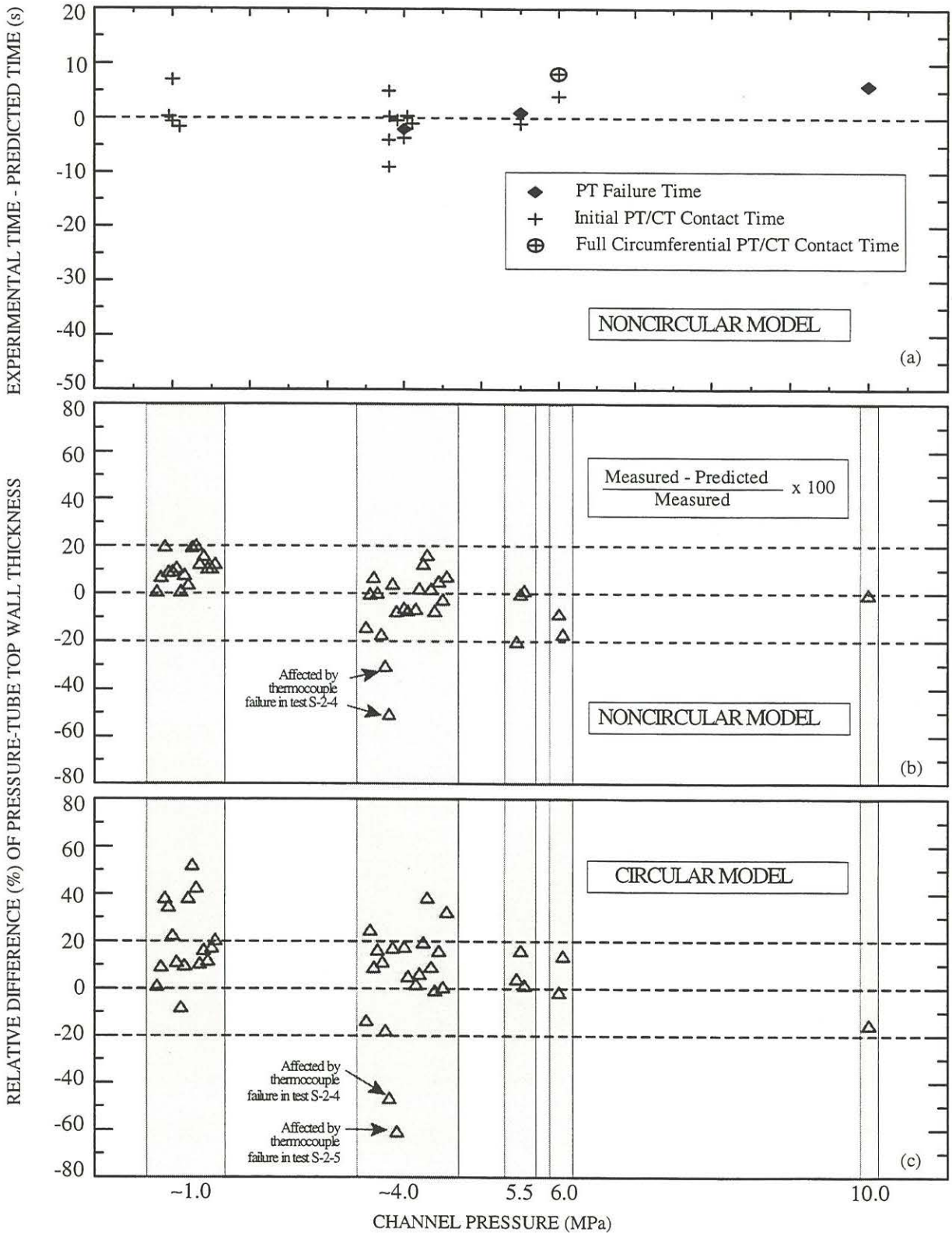

FIGURE 7: Comparisons of Calculated Time (a) and Pressure-Tube Wall Thickness (b) using the Noncircular Model, and Calculated Pressure-Tube Wall Thickness using the Circular Model (c) with Experimental Results (Two data points were removed from (b) and (c) due to effects of heater failure in experiments)